Adsorption of triclosan, trichlorophenol and phenol by high-silica zeolites
Adsorption efficiencies and mechanisms

Jiang, Nan; Shang, Ran; Heijman, Sebastiaan G.J.; Rietveld, Luuk C.

DOI
10.1016/j.seppur.2019.116152

Publication date
2020

Document Version
Final published version

Published in
Separation and Purification Technology

Separation and Purification Technology 235 (2020) 116152

Contents lists available at ScienceDirect

Separation and Purification Technology

journal homepage: www.elsevier.com/locate/seppur

Adsorption of triclosan, trichlorophenol and phenol by high-silica zeolites: Adsorption efficiencies and mechanisms

Nan Jiang*, Ran Shang*, Sebastiaan G.J. Heijman, Luuk C. Rietveld

Section of Sanitary Engineering, Department of Water Management, Faculty of Civil Engineering and Geosciences, Delft University of Technology, P.O. Box 5048, 2600 GA Delft, the Netherlands

ARTICLE INFO

Keywords:
High-silica zeolites
Adsorption
Organic compounds
Water treatment

ABSTRACT

High-silica zeolites can be used for adsorption of organic compounds (OCs) from water. The adsorption efficacy could vary with the properties of OCs, as well as the porous and surface features of high-silica zeolites. In this study, the adsorption of triclosan, trichlorophenol (TCP) and phenol by ten high-silica zeolites were investigated. The plateaus of adsorption isotherms were observed in the adsorption of triclosan. The maximum adsorption capacity of triclosan could be related to the surface area and volume of micropores. The adsorption of TCP by FAU zeolites gave an S-shaped isotherm due to the possible lateral interactions of TCP molecules in the specific pore topology of FAU zeolites. The adsorption of phenol by high-silica zeolites had no adsorption plateau. Zeolites with channel structures, e.g. MFI zeolites, possess closely fitted pores for phenol, which slightly promoted its adsorption efficacy. The active adsorption sites of zeolites, i.e. Brønsted acid sites (BAS) and Lewis acid sites (LAS) failed to promote phenol adsorption. Phenol adsorption was favoured by carbon-based adsorbents with aromatic rings and functional groups, e.g. carboxyl and carbonyl, while the lack of active adsorption sites limited the phenol adsorption by high-silica zeolites, especially at the low concentration range.

1. Introduction

Zeolites are crystalline aluminosilicates with uniform micropores (pore size of less than 2 nm). The porous structure of zeolites is generated from a three-dimensional framework constructed by SiO_4 and AlO_4 tetrahedra [1,2]. The properties of zeolites vary with the Si and Al content in the framework, typically characterized by the silica to alumina molar ratio (Si/Al ratio). Low-silica zeolites (Si/Al ratio < 2) possess a high ion exchange capacity and therefore have been used for water softening [3]. High-silica zeolites (Si/Al ratio up to several thousands) can be synthesized from low-silica zeolites by replacing aluminium with silica [4,5]. High-silica zeolites have been found to be efficient adsorbents for the removal of emerging organic compounds (OCs), e.g. methyl tert-butyl ether (MTBE) [6,7] and N-nitrosamines [8,9], which are hardly adsorbed by activated carbon.

Triclosan, a commonly used antibacterial and antifungal agent, has caused public attention because of its extensive use in personal care products and possible disposal in water [10]. Treatment technologies such as biological treatment [11], oxidation [12,13] and adsorption by activated carbon (AC) [14,15] and carbon nanotubes [16,17] have been used to treat water containing triclosan, while the adsorption of triclosan by high-silica zeolites has not yet been reported in literature.

Phenol and chlorophenol, including 2,4,6-trichlorophenol (TCP) are widely used in the production of industrial commodities and, as a result, have been commonly detected in water bodies [18,19]. The adsorption of TCP and phenol in water by some high-silica zeolites has been previously studied. Zhang. et al. evaluated the adsorption of TCP by FAU type high-silica zeolites. The maximum adsorption capacity could not be determined since an adsorption plateau was not observed [20]. Yang. et al. studied TCP adsorption by FAU zeolites with different Si/Al ratios. As the isotherm curves with linear shape showed, FAU zeolites with higher Si/Al ratios had better adsorption efficacies than zeolites with lower Si/Al ratios. However, TCP adsorption by high-silica zeolites with other framework types has not been studied before. Phenol adsorption by high-silica zeolites with different frameworks, i.e. FAU, BEA, MOR and MFI types, has been studied by Damjanovic et al. [21] and Khalid et al. [22]. The maximum adsorption capacity and its relationship to the properties of high-silica zeolites, occurring at several g L^{-1}, were well elaborated. However, no attempt has been made to provide insight into the adsorption isotherm of phenol at lower and environmentally relevant concentrations, e.g. μg L^{-1}.

The adsorption of specific OCs, e.g. MTBE [6,7,23,24], and OC groups, e.g. N-nitrosamines [8,9] and sulfa drugs [25] in water on high-silica zeolites have been studied in literature. The adsorption efficacy

* Corresponding authors.
E-mail addresses: N.Jiang@tudelft.nl (N. Jiang), R.Shang@tudelft.nl (R. Shang).

https://doi.org/10.1016/j.seppur.2019.116152
Received 11 April 2019; Received in revised form 26 September 2019; Accepted 1 October 2019
Available online 03 October 2019
1383-5866/

and mechanisms of OCs on high-silica zeolites were reviewed by Jiang et al [26]. Based on literature, it was concluded that zeolite properties, such as surface hydrophobicity/hydrophilicity, pore size and structure, affect the adsorption of OCs. The efficacy and mechanism of OC adsorption can also vary based on the properties of OCs, e.g. hydrophobicity/hydrophilicity, molecular weight and size [26]. More research is thus needed to explore the adsorption of representative OCs by high-silica zeolites, which would indicate the OC adsorption mechanisms.

In this study, the adsorption of triclosan, TCP and phenol with the same functional groups, i.e. chlorine atoms and hydroxyls attached to aromatic rings, but also different molecular weight, size and hydrophobicity were selected to represent OCs with diverse properties. The adsorption of three OCs by high-silica zeolites with different porous and surface properties was investigated. The study examined the relationship between the adsorption efficacy of OCs and the properties of both high-silica zeolites and OCs. By comparing the adsorption behaviour of three OCs on various high-silica zeolites, the dominant adsorption mechanisms, i.e. the size/close-fit or the hydrophobicity interaction, could be concluded. Based on these findings, the adsorption efficacies of high-silica zeolites were compared with commonly used adsorbents, e.g. activated carbon, carbon nanotubes and clays.

2. Materials and methods

2.1. High-silica zeolite adsorbents

High-silica zeolite powders of four frameworks, namely FAU, BEA, MOR and MFI, were purchased from commercial companies. The framework types, names, suppliers and Si/Al ratios are listed in Table 1.

2.2. Organic compounds

The analytical standards of triclosan, TCP and phenol were purchased from Sigma-Aldrich, the Netherlands. Their physicochemical properties are listed in Table 2.

2.3. Characterization of high-silica zeolites

Multiple methods were used to characterize the material properties of the high-silica zeolites. BET surface area and pore volume of high-silica zeolites were determined by N_2 gas adsorption at 77 K (Gemini VII 2390p analyzer, Micromeritics). The surface area and volume of micropores (pore size less than 2 nm) were estimated by the t-plot method which separates the micropores from multilayer adsorption of N_2 gas [27,28]. XRF analyses were performed with a Panalytical Axios Max WD-XRF spectrometer to characterize the Si/Al ratio of high-silica zeolites. The data evaluation was conducted using SuperQ5.0i/Omnian software.

Table 1
Names and supplier information of high-silica zeolites.

Framework type	Zeolite name[a]	Product name	Company	Si/Al ratio[b]
FAU	FAU250	390HUA	Tosoh	250
	FAU50	385HUA	Tosoh	50
	FAU40	CBV901	Zeolyst	40
	FAU30	CBV760	Zeolyst	30
BEA	BEA250	980HOA	Tosoh	250
	BEA150	cp811c-300	Zeolyst	150
	BEA75	CZB 150	Clariant	75
MOR	MOR120	690HOA	Tosoh	120
MFI	MFI750	890HOA	Tosoh	750
	MFI45	CZP90	Clariant	45

[a] The zeolite names in this study was composed by the framework type and Si/Al ratio provided by suppliers.
[b] Si/Al ratio provided by suppliers.

Two types of acid sites, i.e. Brønsted acid sites (BAS) and Lewis acid sites (LAS), exist in high-silica zeolites. The BAS are weakly bound protons of a bridging hydroxyl group, typically between silica and aluminium ($-Si-OH^+-Al-$). LAS are formed at the extra framework aluminium species and framework defects of hydrogen-type high-silica zeolites [29]. The number of BAS and LAS were determined by transmission Fourier-transform infrared spectroscopy (FTIR, Nicolet 6700 spectrometer equipped with MCT/B detector) using pyridine as a probe molecule. Zeolite samples were pressed into disks with a radius of 0.8 cm and a weight of 50 mg. The disk was activated in vacuum at 400 °C for 16 h to remove the adsorbed species. After activation, the disk was saturated with pyridine vapour and evacuated at 160 °C for 2 h. The number of BAS and LAS was derived from the bands at 1545 and 1456 cm^{-1} of FTIR spectra. The integrated molar extinction coefficients of BAS and LAS were 1.67 and 2.22, respectively [30]. By assuming that one pyridine molecule is adsorbed on one acid site, the number of BAS and LAS (C_{BAS} and C_{LAS}), was calculated by the following equations:

$$C_{BAS} = 1.88 \times IA(B) \times R^2/W \quad (1)$$

$$C_{LAS} = 1.42 \times IA(L) \times R^2/W \quad (2)$$

where *IA(B)* and IA(L) are the integrated absorbance of BAS and LAS band (cm^{-1}), respectively, R is the radius of zeolite disk (cm) and W is the mass of zeolite sample (mg).

2.4. Adsorption isotherm models

The adsorption isotherms were interpreted using different models. The isotherm constants were determined to estimate the maximum adsorption capacity of OCs and to compare the adsorption efficacy of high-silica zeolites.

The Langmuir model [31] has been widely used to describe monolayer adsorption. The model assumes that each adsorption site can hold only one adsorbate molecule. There is no interaction between molecules adsorbed on neighbouring sites. The equation can be expressed as:

$$q_e = \frac{q_m K_L C_e}{1 + K_L C_e}$$

where q_e is the amount of solute adsorbed per unit weight of adsorbent at equilibrium (μmol g^{-1}), C_e is the equilibrium concentration of the solute in the aqueous solution (μmol L^{-1}), q_m is the maximum adsorption capacity (μmol g^{-1}), and K_L is the constant related to the free energy of adsorption (L μmol^{-1}).

The Freundlich model [32] is an empirical model assuming that as the adsorbate concentration increases, the concentration of adsorbate on the adsorbent surface also increases. The Freundlich model can be applied to the adsorption heterogeneous surfaces and for multi-layer adsorption. The equation can be written as:

$$q_e = K_F C_e^{\,n}$$

where K_F is a constant indicative of the relative adsorption capacity of the adsorbent ((μmol g^{-1})(L μmol^{-1})^n) and n is a constant indicative of the intensity of the adsorption. In this study, Freundlich model was interpreted when the adsorption isotherm did not reach a plateau. The adsorption efficiencies of OCs without adsorption plateau can be compared by simply referring to two constants.

The Langmuir-Freundlich isotherm [33] is a combined form of the Langmuir and Freundlich isotherms. At low equilibrium concentrations, the adsorption represents the characteristics of the Freundlich isotherm, while it predicts a monolayer adsorption capacity by the Langmuir isotherm at high concentrations. The equation can be expressed as:

$$q_e = \frac{q_m K_{LF} C_e^n}{1 + K_{LF} C_e^n}$$

where q_m is the maximum adsorption capacity (μmol g^{-1}); K_{LF} is the

Table 2
The structures and physicochemical properties of OCs.

Name	Formula	Molecular weight (g mol^{-1})	Solubility in water (mg L^{-1})[a]	LogD at pH 6[b]	pka[b]	Molecular size (Å)[c]			Structure
						X	Y	Z	
Triclosan	$C_{12}H_7Cl_3O_2$	289.54	10	5.21	8.8	5.82	3.40	8.68	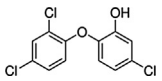
2,4,6-trichlorophenol	$C_6H_3Cl_3O$	197.45	800	3.58	6.2	5.43	0.32	6.28	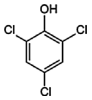
Phenol	C_6H_6O	94.11	$8.28 * 10^4$	1.41	10.0	4.34	0.87	5.55	

[a] Estimated by EPIWEB 4.1.
[b] Estimated by ACD/LABs PhysChem Module (Algorithm Version: 5.0.0.184).
[c] Estimated by Hyperchem 7.0 after geometric optimization.

constant related to the free energy of adsorption (L μmol^{-1}); n is a constant indicative of the intensity of the adsorption. In this study, Langmuir-Freudlich model was used to estimate the maximum adsorption capacity where the adsorption plateau appeared.

2.5. Adsorption experiments

Batch adsorption experiments were conducted in demineralised water. High-silica zeolites (3 mg) were dosed into 100 ml aqueous solution with the varied concentration of 1 to 60 μmol L^{-1} of a single OC solute. After the equilibrium time of 24 h at room temperature (25 ± 1 °C) [21], high-silica zeolites were separated from the solution by membrane filtration (0.2 μm syringe filter, Whatman SPARTAN™).

2.6. HPLC analysis

The concentrations of triclosan, TCP and phenol were determined by HPLC (Shimadzu, Japan) with a C18 column (Phenomenex® KINETEX, 4.6 mm) at 30 °C. HPLC-grade acetonitrile (Sigma-Aldrich, The Netherlands) and ultra-pure water (ELGA, Ultra AN MK2 ultrapure water system) were mixed as the mobile phase. The acetonitrile and water ratios (V:V) were 75:25, 65:35 and 25:75 for triclosan, TCP and phenol, respectively. The flow rate of the mobile phase was 1.0 ml min^{-1}. The wavelength of the UV detector was set at 280 nm.

3. Results

3.1. Characterization of high-silica zeolites

The pores of the high-silica zeolites were characterized by surface area and pore volume and are shown in Table 3. As shown in Table 3, zeolites with a higher surface area had a higher micropore volume. The surface area and pore volume of pores per gram of zeolites of various types followed the order of FAU > BEA > MOR > MFI.

The proportion of micropores accounting for the total pores of high-silica zeolites is shown in Fig. 1. Micropores, which were characterized by micropore surface area and micropore volume, accounted for a large proportion of the zeolite pores. Except for zeolite MFI45, more than 60% of the surface area and 40% of the pore volume were composed by micropores. The surface area and volume of micropores in the FAU zeolites was the highest, while the BEA, MOR and MFI zeolites had a similar but lower surface area and volume of micropores.

The properties relating to the surface chemistry of zeolites can be characterized by Si/Al ratios and acid sites. The results are shown in Table 3. Si/Al ratios of zeolites were both provided by suppliers and determined by XRF, shown in Fig. 2. Except for zeolite FAU250 with a variation of 64%, variations of −28% to 18% were found between the supplier-provided and the XRF-determined Si/Al ratios.

The number of BAS and LAS in the zeolites are shown in Table 3. The variation of BAS and LAS with Al content of zeolites are plotted in Fig. 3. Al content was represented by Al% and expressed by the following equation:

$$Al\% = \frac{Si}{Si + Al}\% = \frac{1}{1 + Si/Al\ ratio}\% \quad (3)$$

As shown in Fig. 3, zeolites had more BAS than LAS. The number of LAS and BAS in FAU and BEA zeolites increased with Al% of zeolites and thus, decreased with Si/Al ratio of zeolites. For example, the number of BAS and LAS in BEA zeolites followed the order of BEA250 > BEA150 > BEA75. No acid sites could be detected from zeolites FAU250 and MFI750 since their Al content was negligible. One exception was the number of BAS in FAU30, which was lower than LAS and also lower than BAS in FAU40. The number of acid sites varied with the framework of zeolites. As shown in Fig. 3, the number of acid sites from BEA, MOR and MFI zeolites was higher than FAU-type zeolites with similar Al content. The effect of Si/Al ratios and acid sites on the OC adsorption efficacy by high-silica zeolites will be further discussed in Section 4.3.

3.2. Adsorption of triclosan by high-silica zeolites

The adsorption isotherms of triclosan by high-silica zeolites were compared in Fig. 4. The maximum adsorption capacity of zeolites were estimated by the isotherm constants of Q_{LF} from Langmuir-Freundlich model (Table 4). The isotherms were not interpreted by Freundlich model since Freundlich model could not estimate adsorption capacity. The adsorption capacity of triclosan varied by the framework type of zeolites. FAU zeolites had a higher adsorption capacity than BEA and MOR zeolites (refer to Q_{LF} in Table 4). The adsorption capacity of MFI zeolites was minimal and therefore excluded from the graph. The adsorption efficacy of triclosan also varied with the properties of high-silica zeolites, e.g. porous properties and Si/Al ratio of zeolites, which will be discussed in Sections 4.2 and 4.5.

3.3. Adsorption of 2,4,6-trichlorophenol (TCP) by high-silica zeolites

As shown in Fig. 4, zeolites with same framework type had the same isotherm shape for triclosan adsorption, although the adsorption capacity of triclosan varied with the framework of zeolites. High-silica zeolites with highest Si/Al ratio of each framework type, namely FAU250, BEA250, MOR120 and MFI750, were thus chosen to study the effect of framework type on TCP adsorption. The adsorption isotherms

Table 3
The structural and chemical characteristics of high-silica zeolites.

Zeolite name	Pore opening size (Å * Å)	Surface area (m^2 g^{-1})	Micropore surface area (m^2 g^{-1})	Pore volume (cm^3 g^{-1})	Micropore volume (cm^3 g^{-1})	Si/Al ratio from XRF analysis	BAS[a] (μmol g^{-1})	LAS[b] (μmol g^{-1})
FAU250	7.4 * 7.4	727	591	0.5136	0.2623	409	N.D.	N.D.
FAU50	7.4 * 7.4	698	571	0.5160	0.2545	43	19	12
FAU40	7.4 * 7.4	606	447	0.4819	0.1966	32	13	17
FAU30	7.4 * 7.4	789	548	0.5233	0.2445	31	133	45
BEA250	6.6 * 7.7 5.6 * 5.6	516	351	0.3022	0.1557	286	16	7
BEA150	6.6 * 7.7 5.6 * 5.6	524	364	0.3243	0.1623	107	54	8
BEA75	6.6 * 7.7 5.6 * 5.6	563	396	0.3720	0.1761	78	85	16
MOR120	6.5 * 7.0 2.6 * 5.7	431	360	0.2687	0.1606	113	52	8
MFI750	5.1 * 5.5 5.3 * 5.6	334	282	0.1702	0.1260	891	N.D.	N.D.
MFI45	5.1 * 5.5 5.3 * 5.6	359	199	0.5341	0.0891	42	142	40

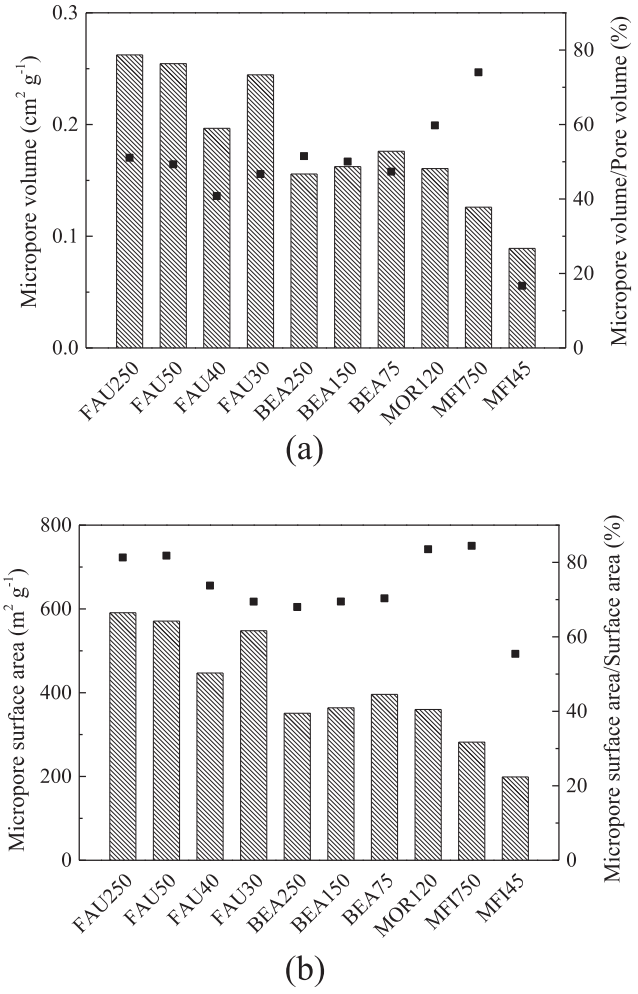

Fig. 1. The proportion of micropores accounting for the total pores of high-silica zeolites. Micropores are represented by micropore volume (the bars in Fig. 1a) and micropore surface area (the bars in Fig. 1b). -■- represent the percentage proportion of micropores accounting for the total pores.

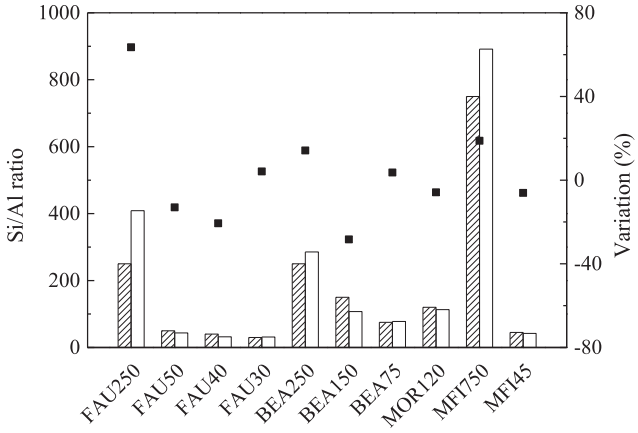

Fig. 2. Comparison of Si/Al ratios given by suppliers (bar with diagonal lines) and measured by XRF analysis (solid bars). -■- is the variation percentage of the XRF-determined Si/Al ratio with the supplier-provided Si/Al ratio.

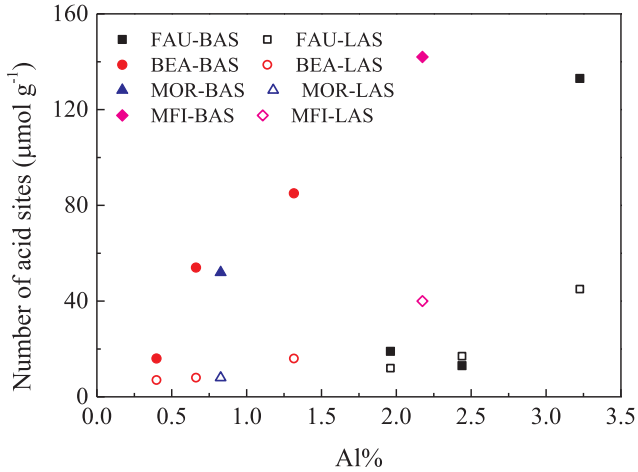

Fig. 3. The variation of BAS (solid symbols) and LAS (open symbols) with Al% of zeolites.

of TCP by FAU250, BEA250 and MOR120 are displayed in Fig. 5. FAU250 was the most efficient adsorbent for TCP in the studied concentration range (0–25 μmol L^{-1}), while the adsorption capacities of BEA250 and MOR120 zeolites were much less than that of FAU250. MFI750 had minimal adsorption of TCP and was therefore not included in the graph.

FAU250 zeolites showed an S-shaped adsorption isotherm with good fitting to the Langmuir-Freundlich model at the concentration range of 0–25 μmol L^{-1} (R^2 = 0.9804, Fig. 5 and Table 5) At the equilibrium concentration range 0–4 μmol L^{-1}, the adsorption capacity reached ~200 μmol g^{-1}, which were well fitted with the Freundlich

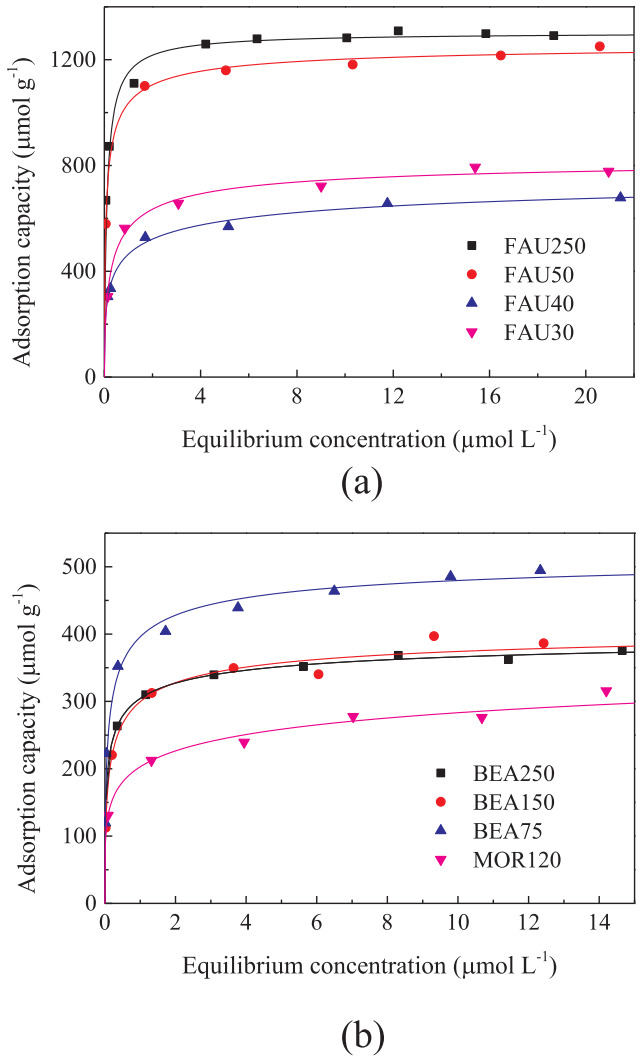

Fig. 4. The adsorption isotherms of triclosan by (a) FAU-type, (b) BEA-type and MOR-type zeolites and the Langmuir-Freundlich model fitting curves (solid lines).

model (isotherm constants, Table 6). The steep slope of the isotherm curve occurred at the equilibrium concentration of about 3.2 μmol L^{-1}. The S-shaped curve reached the plateau with estimated adsorption capacity of 1593 μmol g^{-1} by Langmuir-Freundlich models (Table 5). TCP adsorption by BEA250 and MOR120 zeolites without adsorption plateaus were well fitted with the Freundlich isotherms (Fig. 5). The isotherm constants are given in Table 6.

3.4. Adsorption of phenol by high-silica zeolites

The adsorption isotherms of phenol by high-silica zeolites with different frameworks are shown in Fig. 6. Compared with triclosan and TCP, phenol was adsorbed to a much lesser extent by high-silica zeolites at the same equilibrium concentration range (0–20 μmol L^{-1}). The low adsorption efficacy of phenol was revealed from the low adsorption capacity and the isotherms without adsorption plateaus.

Phenol adsorption by high-silica zeolites was well fitted with the Freundlich isotherm. The isotherm constants are given in Table 7. MFI zeolites exhibited the best phenol adsorption capacity of the tested zeolites. The adsorption efficacy of zeolites followed the order of MFI750 > MFI45 > MOR120 > BEA250 > FAU250 > FAU30, which was in the opposite order of the maximum adsorption capacity of triclosan and TCP (FAU > BEA > MOR, Fig. 4 and Fig. 5).

4. Discussion

4.1. The properties of OCs and their relationship with the adsorption efficacy

The maximum adsorption capacity of an OC was related to the OC size. For example, FAU250 provided a higher adsorption capacity for TCP (1593 μmol g^{-1}, Table 5) than for triclosan (1304 μmol g^{-1}, Table 4), while triclosan is more hydrophobic than TCP. Considering that the pore opening size of FAU zeolites is supposed to be larger than the molecular size of both triclosan and TCP, the adsorption of OCs would happen in the same type of cages with a pore opening size 7.4 Å * 7.4 Å. Since the molecular size of TCP is smaller than the size of triclosan, more TCP molecules could be trapped in one cage, explaining the preferred adsorption in the case of more TCP-molecules in one cage.

Previous studies have shown that the decreased interactions between OC and water will enhance the OC-zeolite interactions, and a strong correlation between the adsorption capacity and hydrophobicity of OCs has been observed [25,34]. In this study, the theory was confirmed by the higher adsorption efficacies of triclosan and TCP than phenol.

4.2. The characterization of high-silica zeolites and their effect on the adsorption capacity of triclosan

The maximum adsorption capacity of triclosan by FAU, BEA and MOR zeolites are observed from the isotherms. The effect of volume and surface area of micropores, pore volume, surface area and Al content on the maximum adsorption capacity of triclosan is shown in Fig. 7 (The effect of Si/Al ratio and Al content, Section 4.5). The maximum adsorption capacity of zeolites (from Langmuir-Freundlich model, Table 3) was more closely correlated to the volume and surface area of micropores than the pore volume and surface area, which indicate that micropores of zeolites dominated the adsorption of triclosan. Compared with the mesopores (pore diameter of 2–50 nm) and macropores (pore diameter of > 50 nm), the size of the micropores (pore diameter of < 2 nm) is closer to the size of the triclosan. Thus, triclosan would experience stronger adsorption forces originating from the “walls” of the micropores.

The micropores of zeolites varied in a range due to their different synthetic processes [35], while zeolites synthesized in the same way could possess similar micropore volume and surface area. In this case, other properties of zeolites, e.g. Al%, could dominate the adsorption efficacy [36]. Moreover, the effect of micropore volume and surface area has not been determined in some studies since the micropores of zeolites were not measured [7,21].

Table 4
Langmuir-Freundlich isotherm constants for triclosan adsorption by different zeolites.

	FAU250	FAU50	FAU40	FAU30	BEA250	BEA150	BEA75	MOR120
Q_{LF} (μmol g^{-1})	1304	1271	825	837	414	420	530	529
K_{LF} (L μmol $^{-1}$)	7.4891	4.3922	1.2865	2.0359	2.7849	2.4775	2.9514	0.6211
n	0.9006	0.5980	0.4157	0.6170	0.4408	0.5142	0.5079	0.2676
R^2	0.9373	0.9929	0.9823	0.9873	0.9864	0.9767	0.9836	0.9647

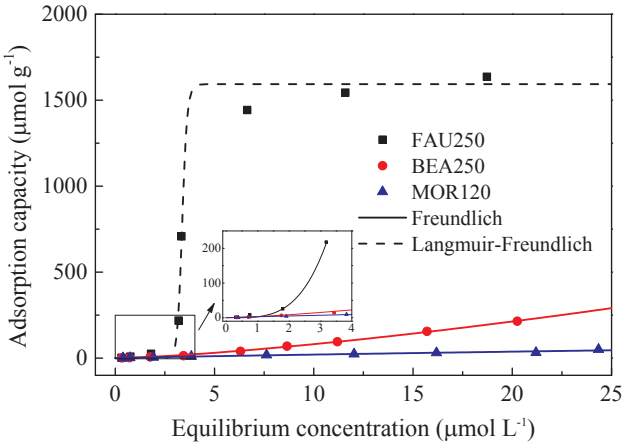

Fig. 5. The adsorption isotherms of TCP by (a) FAU250 and (b) BEA250 and MOR120 and the fitting curves (Solid lines: Freundlich model fitting; Dashed lines: Langmuir-Freundlich model fitting).

Table 5
Langmuir-Freundlich isotherm constants for TCP adsorption by FAU250 zeolite fitting at the equilibrium concentration range of 0–25 μmol L^{-1}.

Q_{LF} (μmol g^{-1})	K_{LF} (L μmol $^{-1}$)	n	R^2
1593	3.92 * E−15	27.26	0.9804

Table 6
Freundlich isotherm constants for TCP adsorption by FAU250 fitting at the equilibrium concentration of 0–4 μmol L^{-1}, BEA250 and MOR120 fitting at the equilibrium concentration of 0–25 μmol L^{-1}.

	FAU250	BEA250	MOR120
K_F (μmol g^{-1}) (L μmol^{-1})^n	2.8621	3.3002	2.7582
n	3.7352	1.3911	0.8720
R^2	0.9970	0.9867	0.9555

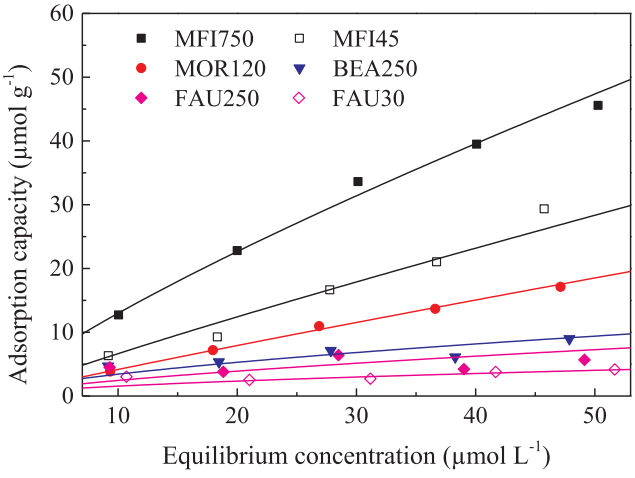

Fig. 6. The adsorption isotherm of phenol by different high-silica zeolites and the Freundlich fitting curves (solid lines).

4.3. The occurrence of the S-shaped isotherm curve

Notably, an S-shaped curve was observed for TCP adsorption by FAU250 zeolite. When the OC intermolecular attraction effects are large, an isotherm with S-shaped is observed [37]. The affinity of TCP for the surface of FAU250 zeolites was low at the starting concentration range of 0–3.2 μmol L^{-1}.(Fig. 5). The pores of high-silica zeolites were

Table 7
Freundlich isotherm constants for phenol adsorption by MFI750, MFI45, MOR120 BEA250, FAU250 and FAU30 zeolites.

	MFI750	MFI45	MOR120	BEA250	FAU250	FAU30
K_F (μmol g^{-1})(L μmol^{-1})^n	2.0350	0.8354	0.4936	0.8097	0.5140	0.3947
n	0.8045	0.9009	0.9265	0.6265	0.6771	0.5939
R^2	0.9937	0.9672	0.9974	0.9233	0.7342	0.9036

then partly filled by TCP molecules. More TCP molecules by experiencing intermolecular attractions could be easily adsorbed, which greatly enhances the adsorption capacity and leads to adsorption saturation [38,39]. The intermolecular attraction might be generated from π-π interactions of TCP benzene rings [40,41].

The occurrence of the S-shaped adsorption isotherm might be attributed to the specific pore topology of FAU zeolites. FAU zeolites possess wide α-cages with an opening size of 7.4 Å * 7.4 Å (Table 3) and an enlarged inner pore diameter 13.7 Å [48], which apparently was able to provide accommodation for more than one TCP molecule. As a comparison, BEA and MOR zeolites possess channel systems. The possible locations of adsorbed OCs in the channels of zeolites are channel intersections with one molecule per intersection [42]. The distance between channel intersections could inhibit the interaction between TCP molecules.

A high Si/Al ratio could also be an essential condition of the S-shaped curve and interaction of TCP. Zeolites with a lower Si/Al ratio might promote water adsorption and weaken the interaction between TCP molecules, as observed by Zhang et al. [20] and Yang et al. [43]. Zhang et al. [20] studied TCP adsorption by FAU zeolites with a lower Si/Al ratio (≥15). At the TCP concentration range 0–150 μmol L^{-1}, which was much higher than the equilibrium concentration in their study, the adsorption isotherm did not show either an S-shaped trend or the adsorption plateau. Yang et at. also applied FAU zeolites with a Si/Al ratio of 40 for TCP adsorption and the adsorption plateau was observed [43].

4.4. Phenol adsorption and close-fit theory

At the studied concentration range, phenol adsorption by MFI zeolites, which have smaller pore sizes than other types of zeolites, was higher than on FAU zeolites, which have larger pore opening sizes and a higher volume and surface area of micropores. The favourable adsorption on MFI zeolites could be attributed to the pore size effect. The pores of MFI zeolites originate from a channel system with opening sizes of 5.1 Å * 5.5 Å and 5.3 Å * 5.6 Å (Table 3), which closely fit phenol molecules with a molecular size of 4.34 Å * 0.87 Å * 5.55 Å (Table 2). Closely fitted pores will promote the adsorption efficacy of OCs by generating stronger adsorption forces between OCs and the "wall" of micropores [44]. Damjanovic et al. found that the heat evolved by phenol adsorption on BEA zeolites was lower than in the case of MFI zeolites with better fitted pores for phenol, thus indicating a weaker interaction [21]. The so-called "close-fit" phenomenon has previously been noted from, e.g. the adsorption of multi-solutes by MOR zeolites, as well as the adsorption of MTBE by MFI zeolites [45]. Giaya and Thompson [46,47] proposed that closely fitted pores would reduce the number of water clusters and that the interaction between OCs and the framework of zeolites would be stronger.

The occurrence of "close-fit" is also influenced by the pore structure. In the channel-based pores, the inner size of pores is the similar to the pore opening size of zeolites. OCs, e.g. phenol, with a fitted size for the pore opening could then enter and well fit the channel, such as those found in MFI and MOR zeolites. However, "close fit" is unlikely to happen in the cage-based pores, e.g. cages of FAU zeolites, since OCs with fitted sizes for the pore opening (7.4 Å) will be somewhat smaller than the size of internal pores (13.7 Å) [48], resulting in an unfavoured

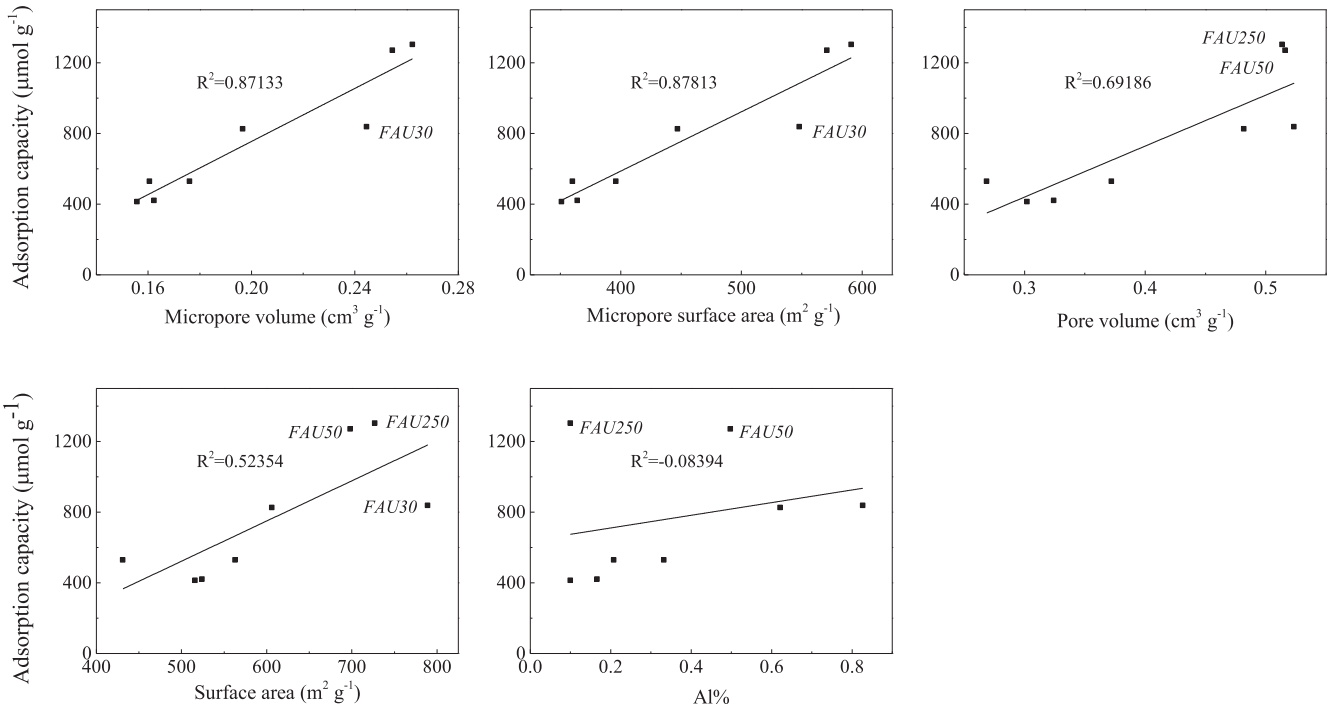

Fig. 7. The correlation between the maximum adsorption capacity of triclosan (estimated from Langmuir-Freundlich isotherms, refer to Table 4) and the properties of high-silica zeolites.

adsorption of phenol by FAU zeolites (Fig. 6).

4.5. Surface hydrophobicity and active adsorption sites of high-silica zeolites

High-silica zeolites feature a high silica content and, thus, a relatively hydrophobic surface. The water affinity for high-silica zeolites was characterized by either Si/Al ratio or the number of acid sites (Table 3).

The effect of Si/Al ratio (Al content) on the adsorption efficacy of high-silica zeolites has been frequently observed. Owing to the highly hydrophobic surface, zeolites with a higher Si/Al ratio (Al content) have shown a higher adsorption capacity of OCs, e.g. nitrobenzene and α-endosulfan [36,49]. The surface hydrophobicity of zeolites, however, had a less pronounced effect on the maximum adsorption capacity of triclosan than the micropore volume and surface area in this study (Fig. 7). Since triclosan is hydrophobic and weakly interacts with water, triclosan adsorption in the pores of zeolites might trigger the water desorption and pore filling by triclosan [21]. Thus, water adsorption that was enhanced by the Al content of zeolites would not affect the maximum adsorption capacity of triclosan.

High-silica zeolites possess a certain number of acid sites (number of LAS and BAS, Table 3) and associated base sites, which might act as active adsorption sites for OCs [50,51]. From Table 3, it can be observed that MFI45 and FAU30 possess over 100 μmol L^{-1} more active adsorption sites than MFI750 and FAU250. However, MFI750 and FAU250, with fewer adsorption sites, showed an enhanced adsorption efficacy over MFI45 and FAU30 of phenol (Fig. 6 and Table 7). Since the active adsorption sites originated from the Al content of zeolites where water clusters preferably gathered, phenol adsorption could experience even stronger water competition at the active adsorption sites than at other adsorption sites [52]. Therefore, phenol adsorption could be inhibited.

A number of silanol groups (Si—OH) exist in the framework of zeolites and are able to adsorb water molecules and polar OCs, such as methanol, by forming H-bonding [53,54]. In addition, Bal'zhinimaev et al. found that the Si—OH groups in FAU250 exist as silanol nests in the cages of the zeolite, while silanol nests in MOR240 are located in the channel entrances [55]. Probably, water molecules interacted with the silanol nests by H-bonding and then formed a strong complex. Since phenol is more hydrophilic and polar than triclosan and TCP, phenol is therefore more likely to be adsorbed on the Si—OH groups by replacing water molecules.

4.6. Comparison with other adsorbents

The adsorption efficacies of triclosan, TCP and phenol by high-silica zeolites and other commonly used adsorbents, e.g. carbonaceous materials and clays, are compared in Tables S1, S2 and S3. When the adsorption plateau was observed, the maximum monolayer adsorption capacity could be estimated by Langmuir and Langmuir-Freundlich isotherms. At the adsorption stage without a plateau, adsorption efficacy was characterized by the K_F value from Freundlich isotherm and the obtained maximum adsorption loading, either given in the literature or recalculated by given experimental data.

In comparison with other absorbents, high-silica zeolites featured a high monolayer adsorption capacity for triclosan (378 mg g^{-1} in Tables S1, translated from the Q_{LF} of FAU250 zeolite in Table 4). The monolayer adsorption capacity of triclosan increased with the pore surface area. Clay adsorbents with a small surface area of pores, e.g. kaolinite and montmorillonite, proved to be less efficient for triclosan adsorption [56]. Benefitting from the hydrophobic surface, high-silica zeolites had the highest K_F value among the reported results (1163 (mg g^{-1})(L mg^{-1})^n, in Tables S1), indicating their high adsorption efficacy at low concentration.

At the low concentration range without the adsorption plateau, carbon nanotubes and graphene showed a high adsorption efficacy too. For instance, carbon nanotubes could achieve an adsorption loading of about 367 mg g^{-1} at the concentration range 0–1 mg L^{-1}. It might be attributed to the surface functional groups of carbonaceous materials, which would provide strong adsorption forces for triclosan [16,56].

FAU250, activated carbon fibers and carbon nanotubes were able to achieve the maximum monolayer adsorption capacity of TCP, which was promoted by surface area (Tables S2). The finding was consistent

with the results of triclosan adsorption. Due to the large number of surface functional groups and the possible condensation of TCP molecules in the pores, carbon nanotubes showed great adsorption efficacy at the low concentration range. Other adsorbents, including AC, failed to reach the adsorption plateau, which indicated their low affinity for TCP adsorption.

With the exception of FAU250 zeolites in this study, S-shaped isotherm curves of TCP adsorption by solid adsorbents were not observed. Regarding the pore topology, TCP interactions are more likely to occur in the uniform micropores of zeolites than in the pores of adsorbents with widely distributed sizes, e.g. AC [57], or in adsorbents with sizes much larger than TCP, e.g. carbon nanotubes with mesopores [58]. For example, Qin et al. [59] studied the adsorption of TCP by SBA-15, a silica based material with mesopores (average pore size 5 nm). The adsorbed TCP molecules were more likely to locate separately in the mesopores, which would not support the intermolecular attraction of TCP.

Compared with high-silica zeolites, phenol adsorption was favoured by carbon-based adsorbents, e.g. activated carbon and AC fibres, as indicated by their high adsorption capacity [60,61]. Roostaei et al. compared phenol adsorption by different solid adsorbents. At the equilibrium concentration of $\sim 120\ mg\ L^{-1}$, the adsorption loading of activated carbon and FAU zeolites were $\sim 268\ mg\ g^{-1}$ and $\sim 17\ mg\ g^{-1}$, respectively [62].

It is well-known that the carbon-based solid adsorbents possess a large number of functional groups as the adsorption sites for phenol, e.g. carboxyl and carbonyl, which would interact with acidic OCs, e.g. phenol [58,61,63]. The aromatic ring of OCs also experience π-π interactions with the carbon surface. Both interactions promote the adsorption efficacy of OCs, especially at a low concentration range [44,64]. The effect of active adsorption sites of high-silica zeolites was less pronounced than the carbon based adsorbents due to lack of organic functional groups in high-silica zeolites and the possible inhibition for phenol adsorption as discussed in Section 4.3.

5. Conclusions

The adsorption efficacy of triclosan, TCP and phenol by high-silica zeolites was studied. The adsorption behaviour and mechanisms were illustrated by various shapes of adsorption isotherms. The adsorption efficacy of OCs by high-silica zeolites was related to the properties of OCs, the porous and surface chemistry features of high-silica zeolites. The conclusions are summarized as below:

- Triclosan and TCP were more favourably adsorbed by FAU-type high-silica zeolites than BEA-, MOR- and MFI-type zeolites. The maximum adsorption capacity of triclosan was related to the micropore volume or micropore surface area of zeolites, rather than the hydrophobicity of the zeolites. The maximum adsorption capacity of FAU250 zeolites for OCs with smaller molecular sizes, e.g. TCP, was higher.
- S-shaped adsorption isotherms indicated the inefficient removal of TCP at low concentrations. The occurrence of an S-shaped isotherm in the TCP adsorption by FAU250 zeolites could relate to the large sized cages of FAU zeolites which allowed the intermolecular attractions between multi TCP molecules. A high Si/Al ratio could also be an essential condition of the S-shaped curve and interaction of TCP.
- Closely fitted pores of high-silica zeolites promoted the adsorption efficacy of phenol, which typically has a low affinity for high-silica zeolites. The occurrence of “close-fit” was more observed with channel-based zeolites, e.g. MFI-type zeolites, compared to cage-based zeolites, e.g. FAU-type zeolites.
- The adsorption of OCs by high-silica zeolites benefitted from the rich amount and closely fitted arrangement of the pores for OCs. Compared with carbon-based materials, the lack of effective active adsorption sites limited the adsorption of phenol by high-silica zeolites, especially at the low concentration range where no maximum adsorption capacity was observed.

Declaration of Competing Interest

The authors declared that there is no conflict of interest.

Acknowledgements

This work is financed by the TKI project Zeotreat. Nan Jiang acknowledges the China Scholarship Council for her PhD scholarship under the State Scholarship Fund (No. 201406120042). The authors acknowledge Prof.dr.ir. Freek Kapteijn and Dr.ir. Irina Yarulina for the measurement of acid sites.

Appendix A. Supplementary material

Supplementary data to this article can be found online at https://doi.org/10.1016/j.seppur.2019.116152.

References

[1] P. Jacobs, E.M. Flanigen, J. Jansen, H. van Bekkum, Introduction to Zeolite Science and Practice, Elsevier, 2001.
[2] S.M. Auerbach, K.A. Carrado, P.K. Dutta, Handbook of Zeolite Science and Technology, CRC Press, 2003.
[3] A.S. Behrman, Recent developments in zeolite softening, Ind. Eng. Chem. 19 (1927) 445–447.
[4] A. Burton, Recent trends in the synthesis of high-silica zeolites, Cat. Rev. 60 (2018) 132–175.
[5] A.W. Burton, S.I. Zones, S. Elomari, The chemistry of phase selectivity in the synthesis of high-silica zeolites, Curr. Opin. Colloid Interface Sci. 10 (2005) 211–219.
[6] D. Knappe, A.R. Campos, Effectiveness of high-silica zeolites for the adsorption of methyl tertiary-butyl ether from natural water, Water Sci. Tech. – Water Sup. 5 (2005) 83–91.
[7] R. Gonzalez-Olmos, F.-D. Kopinke, K. Mackenzie, A. Georgi, Hydrophobic Fe-zeolites for removal of MTBE from water by combination of adsorption and oxidation, Environ. Sci. Technol. 47 (2013) 2353–2360.
[8] Y.Z. He, H.F. Cheng, Degradation of N-nitrosodimethylamine (NDMA) and its precursor dimethylamine (DMA) in mineral micropores induced by microwave irradiation, Water Res. 94 (2016) 305–314.
[9] D.J. de Ridder, J.Q.J.C. Verberk, S.G.J. Heijman, G.L. Amy, J.C. van Dijk, Zeolites for nitrosamine and pharmaceutical removal from demineralised and surface water: Mechanisms and efficacy, Sep. Purif. Technol. 89 (2012) 71–77.
[10] M. Adolfsson-Erici, M. Pettersson, J. Parkkonen, J. Sturve, Triclosan, a commonly used bactericide found in human milk and in the aquatic environment in Sweden, Chemosphere 46 (2002) 1485–1489.
[11] G.-G. Ying, R.S. Kookana, Triclosan in wastewaters and biosolids from Australian wastewater treatment plants, Environ. Int. 33 (2007) 199–205.
[12] S. Suarez, M.C. Dodd, F. Omil, U. von Gunten, Kinetics of triclosan oxidation by aqueous ozone and consequent loss of antibacterial activity: relevance to municipal wastewater ozonation, Water Res. 41 (2007) 2481–2490.
[13] Q. Wu, H. Shi, C.D. Adams, T. Timmons, Y. Ma, Oxidative removal of selected endocrine-disruptors and pharmaceuticals in drinking water treatment systems, and identification of degradation products of triclosan, Sci. Total Environ. 439 (2012) 18–25.
[14] S.K. Behera, S.-Y. Oh, H.-S. Park, Sorption of triclosan onto activated carbon, kaolinite and montmorillonite: effects of pH, ionic strength, and humic acid, J. Hazard. Mater. 179 (2010) 684–691.
[15] Y. Liu, X. Zhu, F. Qian, S. Zhang, J. Chen, Magnetic activated carbon prepared from rice straw-derived hydrochar for triclosan removal, RSC Adv. 4 (2014) 63620–63626.
[16] H.-H. Cho, H. Huang, K. Schwab, Effects of solution chemistry on the adsorption of ibuprofen and triclosan onto carbon nanotubes, Langmuir 27 (2011) 12960–12967.
[17] S. Zhou, Y. Shao, N. Gao, J. Deng, C. Tan, Equilibrium, kinetic, and thermodynamic studies on the adsorption of triclosan onto multi-walled carbon nanotubes, Clean-Soil Air Water 41 (2013) 539–547.
[18] J. Gao, L. Liu, X. Liu, H. Zhou, S. Huang, Z. Wang, Levels and spatial distribution of chlorophenols – 2, 4-dichlorophenol, 2, 4, 6-trichlorophenol, and pentachlorophenol in surface water of China, Chemosphere 71 (2008) 1181–1187.
[19] K. Schmidt-Bäumler, T. Heberer, H.J. Stan, Occurrence and distribution of organic contaminants in the aquatic system in Berlin. Part II: Substituted phenols in Berlin surface water, Acta Hydroch. Hydrob. 27 (1999) 143–149.
[20] Y. Zhang, R.G. Mancke, M. Sabelfeld, S.-U. Geissen, Adsorption of trichlorophenol on zeolite and adsorbent regeneration with ozone, J. Hazard. Mater. 271 (2014) 178–184.
[21] L. Damjanovic, V. Rakic, V. Rac, D. Stosic, A. Auroux, The investigation of phenol

removal from aqueous solutions by zeolites as solid adsorbents, J. Hazard. Mater. 184 (2010) 477–484.
[22] M. Khalid, G. Joly, A. Renaud, P. Magnoux, Removal of phenol from water by adsorption using zeolites, Ind. Eng. Chem. Res. 43 (2004) 5275–5280.
[23] A. Rossner, D.R.U. Knappe, MTBE adsorption on alternative adsorbents and packed bed adsorber performance, Water Res. 42 (2008) 2287–2299.
[24] H.-W. Hung, T.-F. Lin, Adsorption of MTBE from contaminated water by carbonaceous resins and mordenite zeolite, J. Hazard. Mater. 135 (2006) 210–217.
[25] S. Fukahori, T. Fujiwara, R. Ito, N. Funamizu, pH-Dependent adsorption of sulfa drugs on high silica zeolite: modeling and kinetic study, Desalination 275 (2011) 237–242.
[26] N. Jiang, R. Shang, S.G. Heijman, L.C. Rietveld, High-silica zeolites for adsorption of organic micro-pollutants in water treatment: a review, Water Res. (2018).
[27] B.C. Lippens, J.H. de Boer, Studies on pore systems in catalysts. V. The t method, J. Catal. 4 (1965) 319–323.
[28] C. Scherdel, G. Reichenauer, M. Wiener, Relationship between pore volumes and surface areas derived from the evaluation of N_2-sorption data by DR-, BET- and t-plot, Micropor. Mesopor. Mat. 132 (2010) 572–575.
[29] J. Weitkamp, M. Hunger, Chapter 22 Acid and base catalysis on zeolites, in: Studies in Surface Science and Catalysis on Zeolites, 2007, pp. 787–835.
[30] C.A. Emeis, Determination of integrated molar extinction coefficients for infrared absorption bands of pyridine adsorbed on solid acid catalysts, J. Catal. 141 (1993) 347–354.
[31] I. Langmuir, The constitution and fundamental properties of solids and liquids. Part I. Solids, J. Am. Chem. Soc. 38 (1916) 2221–2295.
[32] H. Freundlich, Über die absorption in lösungen, Über Die Adsorpt. in Lös., 1906, pp. 385–470.
[33] R. Sips, On the structure of a catalyst surface, J. Chem. Phys. 16 (1948) 490–495.
[34] B. Koubaissy, G. Joly, P. Magnoux, Adsorption and competitive adsorption on zeolites of nitrophenol compounds present in wastewater, Ind. Eng. Chem. Res. 47 (2008) 9558–9565.
[35] J. Yu, Synthesis of zeolites, Introduct. Zeolite Sci. Practice 168 (2007) 39.
[36] A.H. Yonli, I. Batonneau-Gener, J. Koulidiati, Adsorptive removal of alpha-endosulfan from water by hydrophobic zeolites. An isothermal study, J. Hazard. Mater. 203 (2012) 357–362.
[37] D.M. Ruthven, Principles of Adsorption and Adsorption Processes, John Wiley & Sons, 1984.
[38] C. Hinz, Description of sorption data with isotherm equations, Geoderma 99 (2001) 225–243.
[39] S. Karimi-Lotfabad, M.A. Pickard, M.R. Gray, Reactions of polynuclear aromatic hydrocarbons on soil, Environ. Sci. Technol. 30 (1996) 1145–1151.
[40] C. Janiak, A critical account on π–π stacking in metal complexes with aromatic nitrogen-containing ligands, J. Chem. Soc., Dalton Trans. (2000) 3885–3896.
[41] M.L. Waters, Aromatic interactions in model systems, Curr. Opin. Chem. Biol. 6 (2002) 736–741.
[42] E. Guvenc, M.G. Ahunbay, Adsorption of methyl tertiary butyl ether and trichloroethylene in MFI-type zeolites, J. Phys. Chem. C 116 (2012) 21836–21843.
[43] H. Yang, Y. Hu, H. Cheng, Sorption of chlorophenols on microporous minerals: mechanism and influence of metal cations, solution pH, and humic acid, Environ. Sci. Pollut. Res. 23 (2016) 19266–19280.
[44] F. Su, L. Lv, T.M. Hui, X.S. Zhao, Phenol adsorption on zeolite-templated carbons with different structural and surface properties, Carbon 43 (2005) 1156–1164.
[45] A. Erdem-Senatalar, J.A. Bergendahl, A. Giaya, R.W. Thompson, Adsorption of methyl tertiary butyl ether on hydrophobic molecular sieves, Environ. Eng. Sci. 21 (2004) 722–729.
[46] A. Giaya, R.W. Thompson, Observations on an equation of state for water confined in narrow slit-pores, J. Chem. Phys. 116 (2002) 2565–2571.
[47] A. Giaya, R.W. Thompson, Water confined in cylindrical micropores, J. Chem. Phys. 117 (2002) 3464–3475.
[48] C. Baerlocher, L.B. McCusker, D.H. Olson, Atlas of Zeolite Framework Types, Elsevier, 2007.
[49] J. Reungoat, J.S. Pic, M.H. Manero, H. Debellefontaine, Adsorption of nitrobenzene from water onto high silica zeolites and regeneration by ozone, Separ. Sci. Technol. 42 (2007) 1447–1463.
[50] T. Beutel, M.J. Peltre, B.L. Su, Interaction of phenol with NaX zeolite as studied by 1H MAS NMR, 29Si MAS NMR and 29Si CP MAS NMR spectroscopy, Colloids Surf. A – Physicochem. Eng. Asp. 187–188 (2001) 319–325.
[51] T. Beutel, B.L. Su, Behavior of phenol (phenol–d_5) on NaX zeolite as studied by 1H NMR and FT–IR techniques, Chem. Phys. Lett. 43 (2005) 341–359.
[52] V. Bolis, C. Busco, P. Ugliengo, Thermodynamic study of water adsorption in high-silica zeolites, J. Phys. Chem. B 110 (2006) 14849–14859.
[53] C.K.W. Meininghaus, R. Prins, Sorption of volatile organic compounds on hydrophobic zeolites, Micropor. Mesopor. Mat. 35–6 (2000) 349–365.
[54] I. Batonneau-gener, A. Yonli, S. Hazael-pascal, J. Pedro Marques, J. Madeira Lopes, M. Guisnet, F. Ramôa Ribeiro, S. Mignard, Influence of steaming and acid-leaching treatments on the hydrophobicity of HBEA zeolite determined under static conditions, Micropor. Mesopor. Mat. 110 (2008) 480–487.
[55] B.S. Bal'zhinimaev, E.A. Paukshtis, A.V. Toktarev, E.V. Kovalyov, M.A. Yaranova, A.E. Smirnov, S. Stompel, Effect of water on toluene adsorption over high silica zeolites, Micropor. Mesopor. Mat. 277 (2019) 70–77.
[56] F. Wang, X. Lu, W. Peng, Y. Deng, T. Zhang, Y. Hu, X.-Y. Li, Sorption behavior of bisphenol A and triclosan by graphene: comparison with activated carbon, ACS Omega 2 (2017) 5378–5384.
[57] M. Radhika, K. Palanivelu, Adsorptive removal of chlorophenols from aqueous solution by low cost adsorbent — kinetics and isotherm analysis, J. Hazard. Mater. 138 (2006) 116–124.
[58] G.C. Chen, X.Q. Shan, Y.S. Wang, B. Wen, Z.G. Pei, Y.N. Xie, T. Liu, J.J. Pignatello, Adsorption of 2,4,6-trichlorophenol by multi-walled carbon nanotubes as affected by Cu(II), Water Res. 43 (2009) 2409–2418.
[59] Q. Qin, K. Liu, D. Fu, H. Gao, Effect of chlorine content of chlorophenols on their adsorption by mesoporous SBA-15, J. Environ. Sci. – China 24 (2012) 1411–1417.
[60] R.A. Dobbs, J.M. Cohen, Carbon adsorption isotherms for toxic organics, Municipal Environmental Research Laboratory, Office of Research and Development, US Environmental Protection Agency, 1980.
[61] Q.S. Liu, T. Zheng, P. Wang, J.P. Jiang, N. Li, Adsorption isotherm, kinetic and mechanism studies of some substituted phenols on activated carbon fibers, Chem. Eng. J. 157 (2010) 348–356.
[62] N. Roostaei, F.H. Tezel, Removal of phenol from aqueous solutions by adsorption, J. Environ. Manage. 70 (2004) 157–164.
[63] O. Hamdaoui, E. Naffrechoux, Modeling of adsorption isotherms of phenol and chlorophenols onto granular activated carbon – Part I. Two-parameter models and equations allowing determination of thermodynamic parameters, J. Hazard. Mater. 147 (2007) 381–394.
[64] A. Dabrowski, P. Podkoscielny, Z. Hubicki, M. Barczak, Adsorption of phenolic compounds by activated carbon – a critical review, Chemosphere 58 (2005) 1049–1070.